

An aggregated template methodology: Novel automatic phase-onset identification by template matching

Laure Duboeuf^{1*}, Volker Oye^{1,2} and Ben D. E. Dando¹

¹NORSAR, Gunnar Randers vei 15, Kjeller, Norway, and ²Department of Geosciences, University of Oslo, Oslo, Norway

Received November 2020, revision accepted March 2021

ABSTRACT

The precision of P- and S-wave phase picking strongly determines the precision of earthquake locations, but such picking can be challenging in the case of emergent signals, large data sets or temporally varying seismic networks. To overcome these challenges, we have developed the concept of an aggregated template to perform automatic picking of the P- and S-wave phases. An aggregated template is defined as a representative event for a small area, built by aggregating the best signal-to-noise-ratio seismic traces from events with similar waveforms (i.e. multiplet events). A template matching procedure, based on the cross-correlation between an aggregated template and an unpicked event, automatically determines the unpicked event P- and S-wave phases. This method enables (1) consistent and accurate P- and S-wave phase picking and (2) reduces processing time relative to traditional template matching by using a clustering method that finds the most representative templates for a region, and thus limiting the required number of templates. We established two parameters to weight the picking precision: (1) the cross-correlation between the aggregated template and the unpicked event and (2) the number of P- and S-wave picks determined per event. We tested this method on 2100 events recorded in the south-west of Iceland. Nineteen aggregated templates have been defined and used to automatically pick ~65% of the complete event catalogue with an accuracy within the range of the manual picking uncertainty. These automatically picked events can then be used for event location, even when characterized by low magnitude, low signal to noise ratios and with emergent P-wave signals.

Key words: Data processing, Monitoring.

INTRODUCTION AND MOTIVATION

The development of industrial activities related to fluid injections such as geothermal exploitation (Majer *et al.*, 2007; Zang *et al.*, 2014; Gaucher *et al.*, 2015), carbon sequestration (Goertz-Allmann *et al.*, 2017), or hydrocarbon production (van der Baan and Calixto, 2017) has led to regional and local increases of seismicity rates (Ellsworth *et al.*, 2015; Foulger *et al.*, 2018). For example, the annual number of detected seismic events in the US mid-continent has increased by a fac-

tor of 13, for events with $M_w > 3$, between 1973 and 2015, primarily related to large-scale fluid injections by the hydrocarbon industry (Ellsworth *et al.*, 2015). Similarly, at the In Salah (Algeria) CO₂ sequestration site (Goertz-Allmann *et al.*, 2014) and at the Soultz-Sous-Forêts (France) geothermal field (Rowe *et al.*, 2002), more than 5000 and 16,000 low-magnitude seismic events were detected, respectively. To achieve the seismic monitoring needs at these sites, increasing numbers of sensors are required to be installed. This results in a dramatic growth in the volume of seismic data to process, which inhibits manual processing.

*Email: laureduboeuf@gmail.com

Yet, for any seismological study, accurate and precise locations of seismic events are crucial. A classical way of determining earthquake locations is from the inversion of P- and S-wave arrival times (Geiger, 1910, 1912). In this case, the location precision will be less affected by changes in the network but strongly dependent on the P-wave onset pick accuracy (Pavlis, 1992). Thus, accurately identifying this phase consistently for any given station and event is a fundamental requirement to obtain reliable seismic event locations. The main challenges in obtaining accurate phase picks are related to low signal-to-noise ratios (SNR) and emergent P-wave phases, both of which make P- and S-wave onset identification difficult. This challenge frequently occurs when projects aim to locate and characterize microseismicity (e.g. lower than magnitude 1), using seismological networks with generally too large source-to-receiver distances (Ellsworth, 2013). As there are about ten times more events to analyse for each lower unit of magnitude that is included, large numbers of events will need to be processed. Manual phase picking is then particularly time consuming and impractical for a single analyst. Requiring multiple analysts will likely result in inconsistencies since picking is strongly analyst dependent. Consequently, finding an accurate automatic picking method that performs consistently between events is vital for event processing.

Many different methods to perform automatic picking have been developed, including the use of envelope functions, STA/LTA, high-order statistics, neural networks etc. (see e.g. Ross and Ben-Zion, 2014), which often require a fixed set of parameters, which are applied to a complete data set, regardless of the data heterogeneity. Thus, a form of data homogeneity is a tacit prerequisite to successfully apply such methods. In Iceland, where natural and induced seismicity can be recorded on the same sensor network (Gudhnason, 2014), there is significant waveform diversity that can compromise these classical autopicking methods.

Induced seismicity is often characterized by the repetition of similar events or even by multiplets (seismic events occurring on the same geological structure). This can, for example, be observed at the geothermal field in Soultz-Sous-Forêts, France (Bourouis and Bernard, 2007; Cuenot *et al.*, 2008) and in Basel, Switzerland (Deichmann *et al.*, 2014). Taking advantage of this characteristic, Shearer (1997) exploited the waveform similarities to increase the number of event detections. Templates of representative events, generally called master events, are cross-correlated with continuous seismic data. A high degree of similarity in event location and source mechanism will result in a high cross-correlation coefficient. Thus, once a defined threshold is exceeded, a new event is detected

(Gibbons and Ringdal, 2006; Goertz-Allmann *et al.*, 2014; Kraft and Deichmann, 2014).

Rowe *et al.* (2002) have previously applied cross-correlation detection methods to perform automatic picking on induced events at Soultz-sous-Forêts. They determined new P- and S-picks from the time lags corresponding to the highest cross-correlation coefficient between a master event template and the unpicked event. About 7000 seismic events were successfully repicked, which allowed a location precision improvement and better fracture delineation. However, this method requires events with high SNR on all recorded traces to serve as master event templates. Such events do not necessarily exist in every data set, with events instead exhibiting waveform characteristics similar to Figure 1(d), where there is both a very low SNR across the event and missing seismic traces. In Figure 1(e) and (f), we show examples of events with high SNR on all recording traces, but where many sensors were not operational. This illustrates the idea of a variable seismic network. Data gaps and missing seismic traces caused by instrumentation problems are not uncommon and result in a temporally variable seismic network. Events recorded on only a subset of sensors are not suitable as master event templates. Consequently, finding the required number of master events that are applicable for a complete data set can become very challenging.

To address the problems associated with identifying master events in the presence of both variable signal quality and missing seismic traces, we have developed the concept of an aggregated template (AT). An AT is not a single physical event but a representative earthquake record, constructed by aggregating the best SNR seismic traces from events with similar waveforms that are assumed to occur close to each other. The resulting AT can then act as a proxy master event for use in an automatic picking routine based on template matching. Thus, an AT forms the basis for consistently identifying P- and S-wave onsets in heterogeneous data sets. Since an AT is generated from multiple events, the problem of data gaps and missing sensors is eliminated. In addition, we present an automated method for their generation, avoiding the challenges associated with the manual identification of master events.

In this paper, we first describe how an AT is generated and how it can be applied to automatically pick phase arrivals using template matching. Secondly, we apply this method to automatically repick a seismic data set recorded from the Reykjanes geothermal field (Fig. 1), located in Iceland. Finally, we discuss the results, and the advantages and disadvantages of this method.

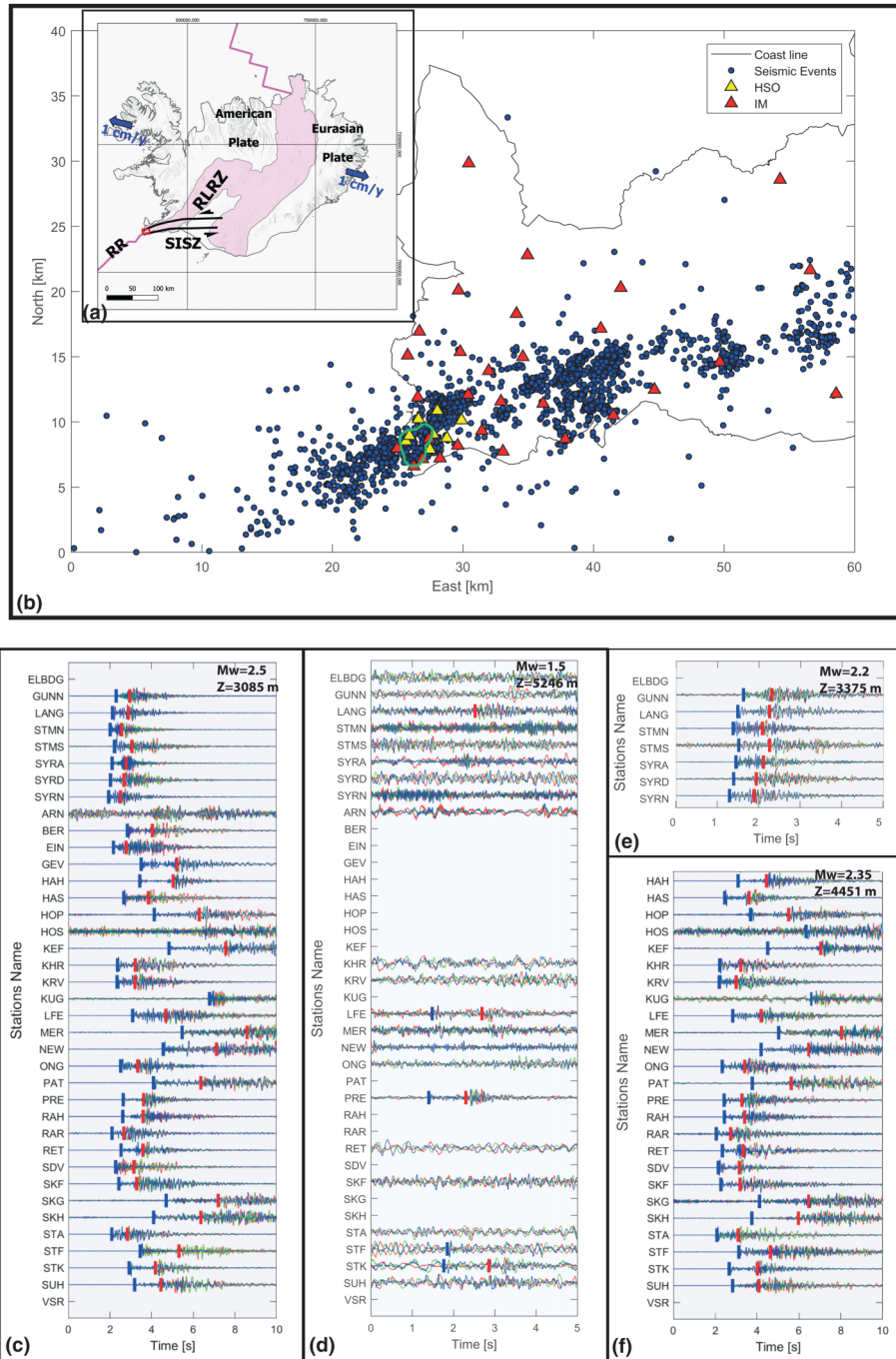


Figure 1 Seismicity map: (a) map of Iceland, showing the plate boundary (pink line), the young volcanic rocks (<0.8 Ma, from Keilegavlen et al., in preparation) and the study area (Reykjanes Peninsula, red square) where the main geological structures (Reykjanes Ridge, South Iceland Seismic Zone – SISZ – and the Reykjanes–Lanagjökull Rift Zone – RLRZ) intersect each other. (b) Zoom on the Reykjanes Peninsula. Red and yellow triangles show the location of the IM (temporary) and HSO (permanent) sensor networks, respectively. The approximate location of the Reykjanes geothermal field (RG) is indicated by the green contour. The blue dots represent the 2160 manually picked earthquake locations. (c–f) Examples of the detected seismic events in or close around the Reykjanes geothermal field. The three channels (E in red, N in green and Z in blue) are superposed. P- and S-picks are symbolized by the vertical blue and orange lines, respectively. (c) An event with a high SNR and only two stations not recording – a potential Master Event candidate. (e) An example of a low SNR event with missing traces and only four clear P-picks – such an event cannot be selected as a master event. (e and f) Two events with high SNR but only recorded on 8 (e) and 25 (f) stations. These events highlight the problem of changing network configuration due to missing seismic traces. These could be selected for the AT process.

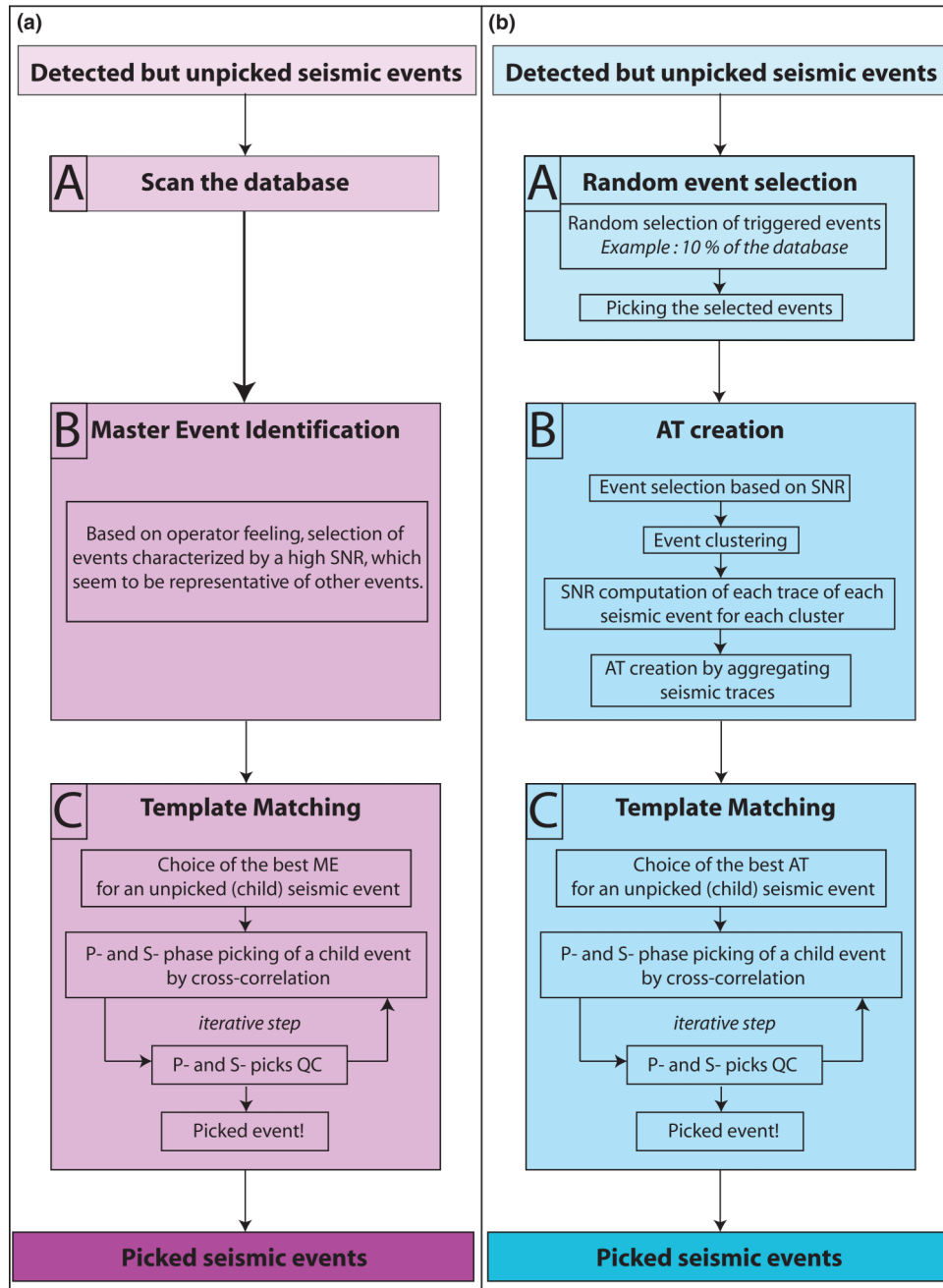


Figure 2 General workflow for automatic P- and S-phase picking using the (a) ME- and (b) AT-based template matching.

GENERATING AGGREGATED TEMPLATES AND THEIR APPLICATION TO AUTOMATIC PHASE PICKING

In Figure 2, we show the overall workflow for automatic phase picking using both traditional master events (MEs) and aggregated templates (ATs). The most significant difference between

the two methods occurs in the formation of the templates (see boxes A and B in Fig. 2).

A prerequisite in creating ATs is a set of seismic events that have been detected using a predefined triggering procedure. Once a set of ATs have been created, the automatic picking methodology can then be applied to either previously detected ‘triggered’ events or non-triggered continuous

seismic data, with both resulting in a set of events with picked P- and S-wave arrivals.

The three main steps (Fig. 2b) required to automatically determine P- and S-wave phases of unpicked seismic events (termed ‘child events’ in this paper) using ATs are:

- A. Random event selection
- B. AT creation
- C. Template matching

Random event selection

Using an initial set of detected but unpicked events, we extract a random selection irrespective of waveform characteristics such as signal-to-noise ratio (SNR). The goal is to gather a subset of events that have the waveform characteristics to be representative of the complete data set and that together constitute enough high SNR traces to be used in a set of aggregated templates. Each of the randomly selected events must subsequently be picked, either manually, or using an automatic phase picker such as AR-AIC (Sleeman and van Eck, 1999). In the case of missing stations or low SNR, these traces can be safely ignored with only valid picks further considered in the creation of the aggregated templates. To ensure that enough representative events are selected, this stage and the subsequent workflow may be run multiple times to ensure all triggered events are ultimately picked.

Aggregated Template Creation

Overview of an Aggregated Template

ATs are an alternative to traditional master event templates and account for data sets characterized by low SNR events and a temporally varying sensor network. Seismic waveforms are strongly dependent on both the seismic ray travel path and the source mechanism of the event. Consequently, events with similar waveforms are considered to have occurred close to each other and to have been induced by similar physical and mechanical processes. Such events can be gathered into multiplet families, which we define here as clusters. An AT is built by selecting the seismic trace with the highest SNR for each station, based on events from a given cluster. Thus, an AT is representative of its cluster of events and should enable the identification of the P- and S-wave onsets for events occurring in this specific area using cross-correlation. The trace aggregation method has two main advantages over traditional template events (i.e. master events). Firstly, for each station and region, the selected seismic trace has the highest possible SNR available in the data set, which maximizes the degree of similarity between the AT and the newly identified highly cor-

related events (child events), due to the lack of noise contamination. Secondly, the AT is generally well represented with seismic traces on all stations, unaffected by potential instrument problems or data gaps.

Three steps are required to construct a successful set of ATs:

- Initial event selection
- Event clustering
- Final event selection and aggregation into a common template

Initial event selection

Each AT must have a high SNR for each of its identified P- and S-wave phases. We therefore select events where the mean SNR is above a defined threshold (e.g. >1). Furthermore, we provide an additional constraint using the percentage of phase picks relative to the number of functioning stations, which helps to ensure that the overall pick quality is high (e.g. see Table 1 for example parameters). This is conceptually demonstrated in Figure 3(a). With an example selection criterion of a mean SNR > 1 and a pick percentage of >50% for the P-wave and >30% for the S-wave, only the event in Figure 3(a4) would not be selected due to the low mean SNR (1) and the low pick percentage of both the P- and S-waves.

Event clustering

Since an AT should be representative of events occurring within a certain area, we have developed a clustering method based on a composite cross-correlation method between stations, and a composite time measure that uses the differential S–P time between pairs of events at a common station. This enables event clustering without requiring event locations.

To ensure that waveform similarity is considered during the clustering, we define a geometric average cross-correlation coefficient composite correlation measure (CM). For a given pair of events (*i, j*), the CM first combines the cross-correlation (*C*) of the P-wave at a single station (STA1), with the cross-correlation of the S-wave at the same station using the geometrical mean

$$C_{ij}^{STA1} = \sqrt{P C_{ij}^{STA1} \times S C_{ij}^{STA1}} \tag{1}$$

The mean cross-correlation can then be combined for two stations using

$$C_{ij} = \sqrt{C_{ij}^{STA1} \times C_{ij}^{STA2}} \\ = \sqrt[4]{P C_{ij}^{STA1} \times P C_{ij}^{STA2} \times S C_{ij}^{STA1} \times S C_{ij}^{STA2}} \tag{2}$$

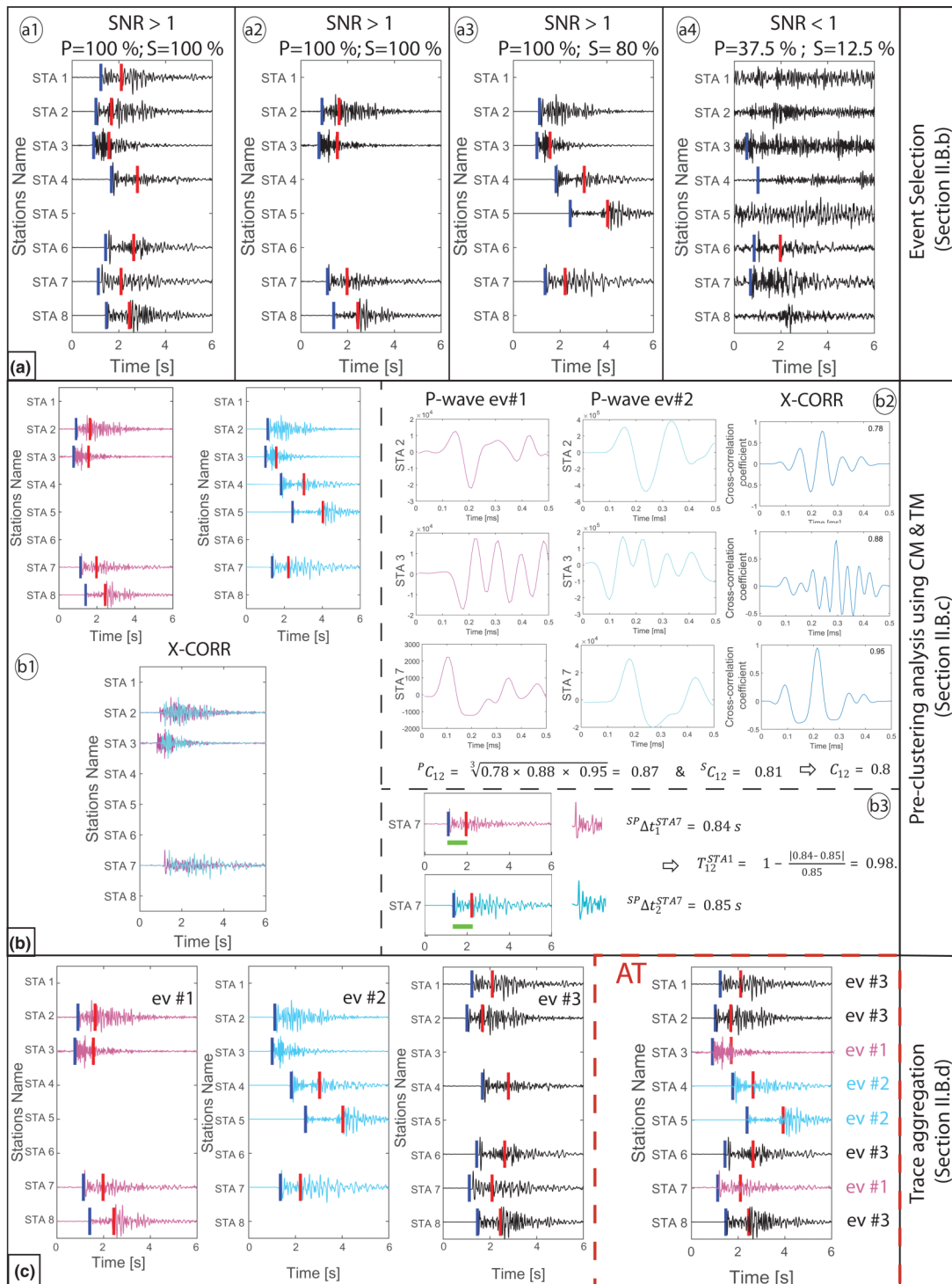


Figure 3 Illustrative example of the steps involved in creating the aggregated templates (e.g. see block B, Fig. 2b). (a) Different randomly selected events that have been subsequently picked for consideration as candidates for the ATs. (b) Illustration of the computation of the CM and TM values, which are used as input for the event clustering. (b1) Two events (pink and blue) where the common traces are cross-correlated. The P-wave cross-correlation function and the maximum cross-correlation coefficient for each trace are shown in (b2), which are used to compute the CM. (b3) The process of computing TM, for a single station 7 and pair of events. The high (CM; TM) couple of (0.8; 0.98) indicate these events will belong in the same cluster. (c) An example of an aggregated template (AT) formed from three events from the same cluster.

Table 1 Parameters to set for using AT methodology

Main part of the workflow	Subpart of the workflow	Parameters to set	Section in the text			
			Theory	Example	Example values in our data set	
AT creation	Initial event selection	SNR	II.B.b	IV.A	>1	
		% of P- and S-picks per event	II.B.b	IV.A	For P-wave phase >50%	For S-wave phase >30%
	Event clustering	Cross-correlation windows for P- and S-wave picks: number of seconds before and after the pick	II.B.c	<i>Not given in the text</i>	For P-wave phase 0.1 s before 0.4 s after	For S-wave phase 0.1 s before 0.6 s after
		(CM; TM) couple	II.B.c	IV.A	> (0.9; 0.8)	
Template matching	Choice of the best AT for an unpicked seismic event	Number of stations used for computing the average cross-correlation coefficient	II.C.a	IV.B.c	8	
		P- and S-phase picking if an unpicked event by cross-correlation	II.C.b.(1)	<i>Not given in the text</i>	For P-wave phase 0.05 s before 0.3 s after	For S-wave phase 0.1 s before 0.6 s after
	Minimum cross-correlation coefficient threshold for considering the P- and S-automatic picks as good	II.C.b.(2;3)	IV.A	For P-wave phase 0.75	For S-wave phase 0.7	
		Maximum distance between two stations to consider them as close (depend on the network)	II.C.b.(2)	<i>Not given in the text</i>	3000 m	

Thus, the general form of the composite CM for M stations, for a given pair of events (i, j) is

$$CM_{ij} = \sqrt{\prod_{k=1}^M {}^P C_{ij}^k \times \prod_{k=1}^M {}^S C_{ij}^k}, \quad (3)$$

where ${}^P C_{ij}^k$ is the cross-correlation coefficient for the event pair (i, j) at station k and for the P- or S-waves and M is the maximum number of sensors.

To perform the cross-correlation, we first filter the data between 2 and 30 Hz, and select windows around the P-wave and the S-wave for which to perform the cross-correlation (see Table 1 for details). An example of the cross-correlation for

a single pair of events recorded on three common stations is shown in Figure 3(b1, b2).

To ensure that the clustering considers distances between pairs of events, we use a composite time measure, TM, that uses the geometric mean of the differential S–P times for pairs of events, based on Stuermer *et al.* (2011, 2012). For a single station ($STA1$), the normalized differential S–P-wave travel-time (T_{ij}^{STA1}) between two events (i, j) is defined as

$$T_{ij}^{STA1} = \left[1 - \frac{|{}^{SP} \Delta t_i^{STA1} - {}^{SP} \Delta t_j^{STA1}|}{\max({}^{SP} \Delta t_i^{STA1}, {}^{SP} \Delta t_j^{STA1})} \right], \quad (4)$$

where ${}^{SP}\Delta t_i^{STA1}$ is the S–P travel-time for event i at station STA1. Thus, T_{ij}^{STA1} will give values of 1, where the S–P travel-times are identical for each event pair and be closer to 0 for large S–P travel-time differences. An example is shown in Figure 3(b3).

We can further combine the normalized differential travel-time for two separate stations (STA1, STA2) using their geometric mean:

$$T_{ij} = \sqrt{\left[1 - \frac{|{}^{SP}\Delta t_i^{STA1} - {}^{SP}\Delta t_j^{STA1}|}{\max({}^{SP}\Delta t_i^{STA1}, {}^{SP}\Delta t_j^{STA1}, {}^{SP}\Delta t_i^{STA2}, {}^{SP}\Delta t_j^{STA2})} \right]} \times \sqrt{\left[1 - \frac{|{}^{SP}\Delta t_1^{STA2} - {}^{SP}\Delta t_2^{STA2}|}{\max({}^{SP}\Delta t_i^{STA1}, {}^{SP}\Delta t_j^{STA1}, {}^{SP}\Delta t_i^{STA2}, {}^{SP}\Delta t_j^{STA2})} \right]}. \quad (5)$$

In generalized form, for M stations, we can simplify this to

$$TM_{ij} = \sqrt{\prod_{k=1}^M \left[1 - \frac{|{}^{SP}\Delta t_i^k - {}^{SP}\Delta t_j^k|}{t_{\text{norm}}} \right]}, \quad (6)$$

where ${}^{SP}\Delta t_i^k$ is the differential travel-time between the S- and P-wave phases observed at station k for event i , and t_{norm} is the maximum S–P time for all of events.

The closer CM and TM are to 1, the more similar the events' waveforms are and the closer their event locations should be, making them ideal metrics for the identification of multiplet events. The method is independent of the event locations and the velocity model, but strongly dependent on P- and S-wave picks. Thus, there is a prerequisite to precisely pick the P- and S-wave arrivals prior to the clustering. Since the clustering is performed using only events characterized by a high SNR from the previous selection of candidate events, the risks of inaccurate picks are minimized. To define each cluster, we first set a threshold for the (CM; TM) couple (e.g. 0.8; 0.9), and only consider event pairs above this threshold. Thereafter, we use a depth-first search algorithm based on the TM values to identify different event clusters.

Template creation by seismic trace aggregation

For each event within a cluster, the SNR is computed separately for each seismic trace. An AT is then built by aggregating the seismic traces with the highest SNR for each station. This process is repeated for each cluster, so the number of ATs is equal to the number of clusters. In Figure 3(c), we show an

example of this process, where the traces from three events are aggregated into a single template.

Automatic picking using template matching

Once a set of ATs have been created, they can then be used to accurately and automatically pick the P- and S-wave onsets of unpicked events (child events) using template matching. The

three main steps involved in the template matching (as outlined in Fig. 2b) are (a) selecting the best matching AT for a child event, (b) automatic picking of the P- and S-wave phases of the child event and (c) quality control of the picked phases.

Selecting the best aggregated template for a child event

The subsequent automatic picking is based on the cross-correlation between an AT and a child event. Thus, identifying which AT has the highest similarity with the child event is the basis for selecting the most appropriate template to generate the automatic picks. For each child event, we determine a mean cross-correlation coefficient for each AT. However, to ensure that the mean cross-correlation best represents the degree of similarity between the child event and AT, we use only the N highest cross-correlation coefficients in the averaging. The choice of N is based on the number of stations that are most frequently operational throughout a data set. We use this approach instead of averaging over all active stations to minimize the risk of poor SNR traces in the child event drastically reducing the mean. The AT with the highest mean cross-correlation coefficient is considered to be the most similar to the child event and selected to perform the automatic phase picking.

Automatic picking

Once an AT is selected, a child event's P- and S-wave phases can be automatically picked. This procedure is split into a further 4 main steps: (1) defining the P- and S-wave time windows, (2) picking the P-wave phases, (3) picking the S-wave

phases and (4) performing an automatic QC on the picked phases to remove potential outliers.

(1) For each trace of the selected AT, we define a constant time window around the P- and S-wave onsets that have already been picked (Fig. 4a). For the unpicked child event, we define a start and end time of the event using an STA/LTA threshold on the stacked envelope of the traces (Fig. 4b), which we then prepend with a small time buffer to equal to the length of the AT P-wave window, to ensure we capture the start of the P-wave. The start of the P-wave window is given by this event start time. We define the end of the P-wave window by finding the maximum amplitude of the envelope, which we assume to be the maximum S-wave amplitude, then limit our window to 90% of the full duration from the window start to this maximum amplitude (Fig. 4c). This helps to avoid the S-wave onset existing within the P-wave window, while still ensuring enough P-wave coda to be beneficial for the template matching.

(2) For each sensor, the P-wave window of the child event is cross-correlated with the P-wave window of the AT (Fig. 4d). The P-wave arrival time pick for the child event is then determined from the time lag obtained for the maximum cross-correlation coefficient. To reduce the risk of inaccurate P-wave picks, we implement an automatic quality control procedure based on the standard deviation of the time lags for a given child event. Where the standard deviation exceeds 20% of the mean, we consider the event to contain P-wave pick outliers. To identify the individual outliers, we use a threshold of plus or minus 1 second from the median, removing any picks that exceed this threshold. A new P-wave window is then defined using the remaining P-wave picks, with the cross-correlation repeated on the traces with missing picks, with the process iterated until the standard deviation decreases to below 20% of the mean.

As a final refinement of the P-wave picks, we apply the method of De Meersman *et al.* (2009). Stations are first grouped together based on a predefined distance criterion. For each group, the seismic traces are aligned on the previously determined P-wave picks and stacked to define a pilot trace. This pilot trace is then cross-correlated with each trace in the group. The P-wave phases are repicked from the time lag obtained for the maximum cross-correlation coefficient between the pilot trace and the child event.

(3) To find the S-wave onsets, we first define an S-wave window, which starts at the time of the P-wave pick plus twice the duration of the AT P-wave window and finishing at the end of the event as defined by the STA/LTA threshold run on the stacked envelope. The same procedure for the P-wave phase

picking is then applied to estimate the S-wave phases, with the exception of the pick refinement method of De Meersman *et al.* (2009), which is not applied due to lack of stability.

(4) The final step in the automatic P- and S-wave phase picking is an automatic quality control to remove potentially incorrect phase picks. The S–P time differential ($t_s - t_p$) is computed for both the AT and the child event. At a given station, these values should almost match. Where there are significant differences based on *a priori* uncertainties for the P- and S-picks, these incoherent P- and S-wave picks are removed.

CASE STUDY CONTEXT: REYKJANES GEOTHERMAL FIELD IN ICELAND

Our study area is the Reykjanes Geothermal System, located at the southern point of the Reykjanes Peninsula, Iceland (Fig. 1a). This area is a complex geological system and is characterized by a transition from the off-shore parts of the Reykjanes Ridge towards a transform zone on land (Björnsson and Einarsson, 1974; Thordarson and Larsen, 2007; Jakobsdóttir, 2008). This constellation results in one of the most seismically active parts of Iceland. Recent volcanic activity accounts for the presence of young magmatic rocks (<0.8 Ma) as well as the unusually high temperature of 320°C at 3 km depth and 427°C at 4.6 km (Khodayar *et al.*, 2018). Such high temperatures allow for geothermal energy exploitation, which in turn is also the source of the induced seismicity, along with the natural, tectonic seismicity.

From mid-March 2014 to mid-August 2015, the seismic activity was recorded by 38 three-component surface geophones (Blanck *et al.*, 2019), of which 8 belong to a permanent network and 30 to a temporary network (called HSO and IM, respectively; Fig. 1b). The still operational HSO 8-sensor network consists of short-period LE-3Dlite geophones, which was run by Iceland GeoSurvey (ÍSOR) on behalf of the geothermal power plant company HS Orka (Weemstra *et al.*, 2016) until 2018, and is located on the top of the Reykjanes geothermal field. The temporary IM network was deployed in the context of the European Union project IMAGE (Weemstra *et al.*, 2016; Blanck *et al.*, 2019) and covered the whole Reykjanes Peninsula. From the 30 stations, 20 were Trillium Compact Broadband seismometers and 10 were short-period Mark L-4C seismometers (Jousset *et al.*, 2016). Both the sensor diversity and the interstation distances (from 0.5 to 40 km) increase the network resolution and allow the recording of both small and large earthquakes at a range of

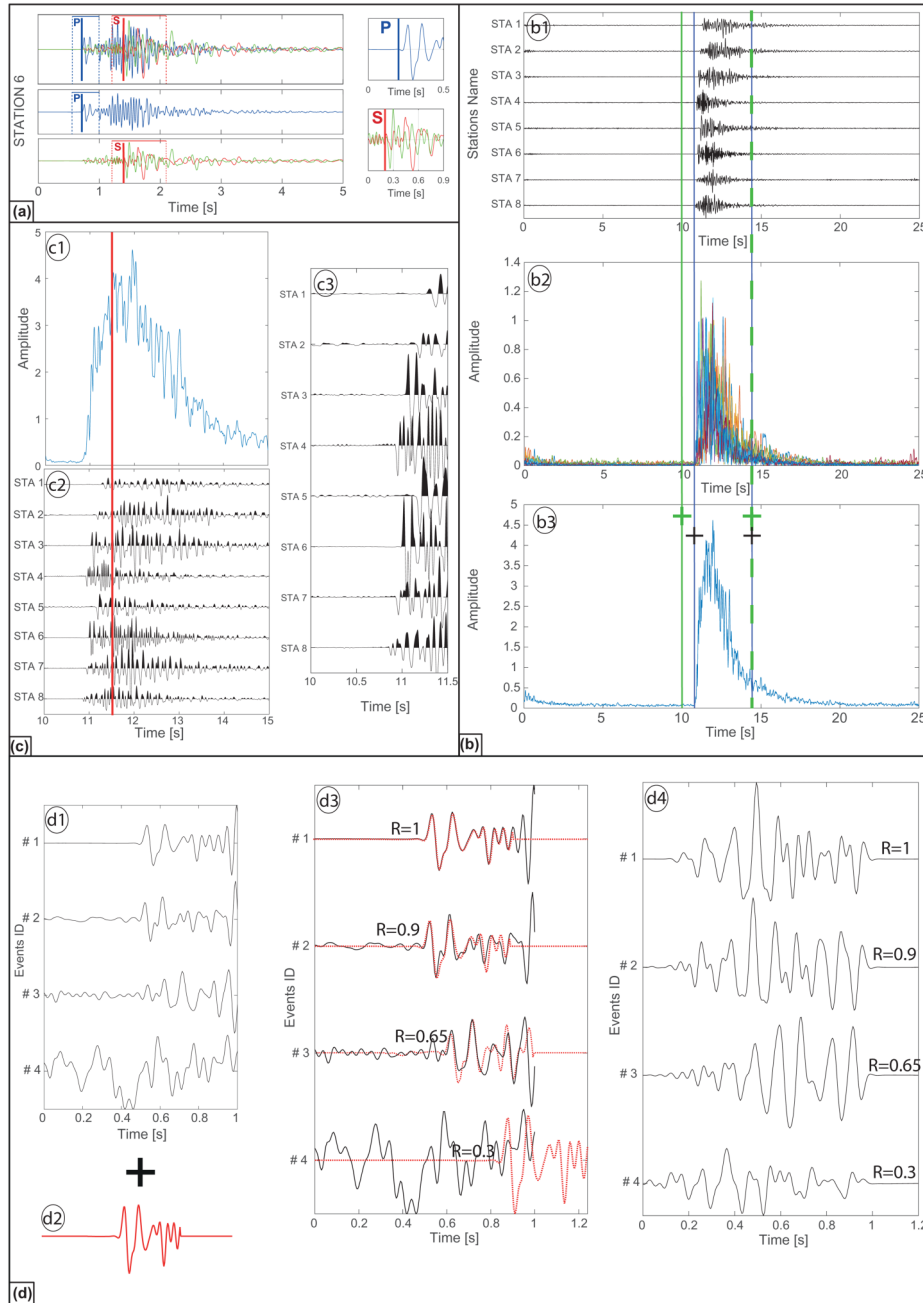


Figure 4 Definition of (a) AT P- and S-windows, (b) child event time duration and (c) P-wave window used to determine the best-fitting AT. (a) The P- and S- windows definitions around the P- and S-onsets for a single AT, for the station STA6. (b) Different steps needed to estimate the child event duration. (b1) Stacked seismic traces of the three components for seven individual stations. For each of those traces, an envelope is computed using a Hilbert transform (b2). Finally, a stacked envelope is computed (b3). The blue crosses and lines indicate the automatic detection of the beginning and the ending of the event determined via a STA/LTA threshold, whereas the green crosses and lines show an extended window around it, required for further analysis. The start of the green window is used as the start of the P-window. (c) The basis for determining the end of the P-wave window. The maximum amplitude of the envelope (c1) is used as an approximation of the S-wave, with the P-wave window end defined at 90% of the duration from the start of the window to the maximum amplitude (c2). The selected P-wave window is shown on c3. (d) Results of the cross-correlation for four child events (d1) with the AT (d2) for the station SYRA. (d3) The superposition of the child events (black traces) with the AT (red dashed traces) and their corresponding cross-correlation coefficient (R).(d4) The cross-correlation function associated with the described process (d1, d2 and d3).

distances. The presence of both induced and natural seismicity in combination with instrument outages increases the database complexity and justifies the use of the aggregated template methodology. An STA/LTA triggering method applied on the continuous seismic data from the two seismic networks during three months in 2015 leads to the detection of more than 6500 earthquakes.

RESULTS

Based on a random selection of the 6500 events, we manually picked 2160 events that occurred from mid-May to mid-August 2015, with an uncertainty visually estimated to be 50–100 ms for the P-wave picks and 150–200 ms for the S-wave picks. At least four P-wave onsets and one S-wave phase were picked per event. These events were repicked applying the aggregated template (AT) methodology and the results compared with the manual picks.

Aggregated Template Creation and Autopicking

After picking the subset of events from the complete set of triggered data, we selected suitable events for the ATs by applying thresholds based on the percentage of P-wave picks (50%), S-wave picks (30%) and the mean signal-to-noise ratio (SNR) of traces (>1) (see Table 1). The SNR generally decreases with an increase in event-station distance while the percentage of picks per event decreases with event magnitude. Consequently, the large event-station distances (up to 80 km) result in few P- and S-wave picks for most of these events. The application of these thresholds left a total of 650 events from the 2160 initially selected and manually picked events.

Figure 5 illustrates the results of the composite correlation measure (CM) and the composite time measure (TM) for each event pair from the 650 events, and the subsequent clustering that is applied. The CM–TM distribution (Fig. 5a) shows that most of the event pairs (red dots) have CM and TM coefficients varying from 0.75 to 0.85 and from 0.65 to 0.75, respectively. Two hundred and fifty event pairs (within the green box, Fig. 5a) present higher similarities ($CM > 0.9$) with smaller travel-time differences ($TM > 0.8$). These represent 143 highly correlated individual events that when located are well distributed along the whole peninsula (green dots on Fig. 5b). Applying the TM-based clustering, which is independent of any event location, which is only shown for illustrative purposes, leads to the definition of 19 different clusters of multiplet events, enabling the formation of 19

different ATs. Each cluster is characterized by strong waveform similarity, as illustrated by the 10 events of cluster no. 1 for the SYRA station (Fig. 5c). The depth distribution of these clusters (Fig. 5d, e) is presented within two cross-sections AA' and BB' (Fig. 5b). From the 19 clusters, 10 are located within the geothermal field (highlighted by the red ellipse) and which are almost overlapping spatially, indicating that only minor differences separate the different ATs. This should result in better identification of the P- and S-wave phases for child events since there is likely to be a template that is highly similar.

From these 19 clusters, 19 ATs were created. Two examples of these 19 ATs, from cluster no. 1 (as shown in Fig. 5c) and no. 14, are presented in Fig. 6. Both ATs show that several events (3 and 6 events, respectively) are used to create the ATs but also that single events dominate their makeup (event #6752 and event #6788, respectively).

To assess the performance of the autopicking via template matching, we used the 19 ATs to pick the 2160 events that had already been manually picked, rather than the complete unpicked data set, which would be the typical application. P- and S-wave onsets are picked only when their respective cross-correlation coefficient at a station is greater than 0.75 and 0.7 (Table 1). Thus, 1375 seismic events, or 63.5% of the database, were automatically picked, with a minimum of four P-wave picks and one S-wave pick per event. Three automatically picked events are shown as examples in Fig. 7.

Autopicking results

Analysis of the number of P- and S-wave picks

The automatic process determines between 4 and 34 P-wave onsets and between 1 and 31 S-wave onsets per event. Primarily due to power outages and other technical issues, the number of recording seismic traces changes throughout the monitoring period. In order to derive a consistent quality estimate, we compute the percentage of P- and S-wave phases picked with respect to the number of available seismic traces. The proportion of stations with picks in the data set (either manually made or derived from the aggregated template (AT) processing) varies from 10% to 100% for P-waves and from 3% to 90% for S-waves. Figure 8(a, b) shows that in cases where more than 25% of P- and S-wave picks were determined, the number of valid picks follows a similar trend for both the AT and the manual picks. For smaller percentages of determined phase picks, the AT method finds fewer

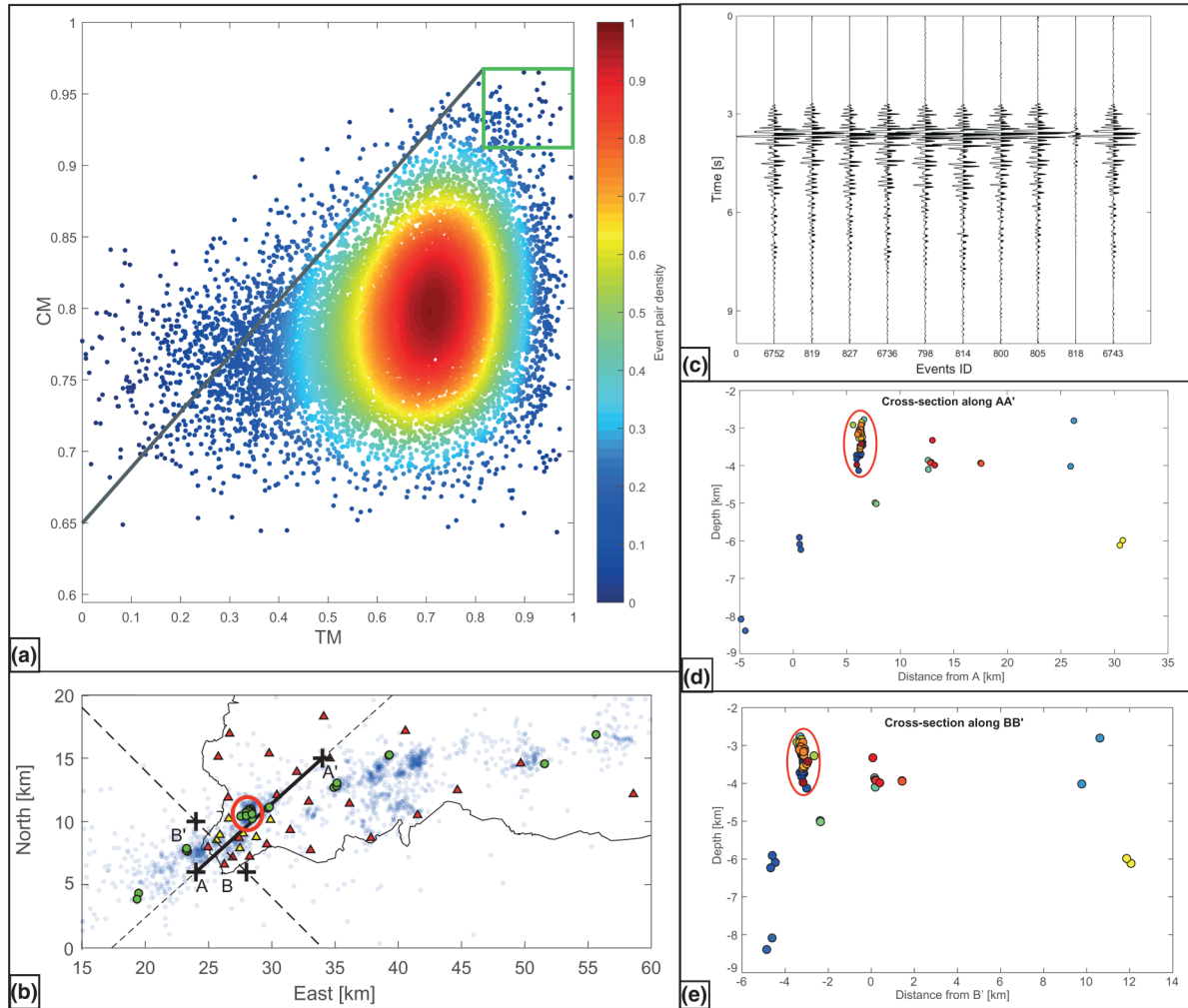


Figure 5 Pre-clustering event-pair analysis and cluster results used to define different ATs. (a) Normalized CM versus normalized TM. Each coloured dot represents a couple (CM; TM) for an event pair for all sensors. The colour indicates the normalized event pair density. The candidate event pairs all show high waveform similarity with no CM values lower than 0.6. The green rectangle indicates the event pairs selected as suitable AT candidates: $(CM; TM) \geq (0.9, 0.8)$. The TM value is subsequently used as input to a clustering algorithm. (b) A zoom-in of Figure 1(b), where the green dots indicate the selected events used to create the ATs and the locations of cross-sections AA' and BB' are shown. (c) Waveforms for 10 different seismic events recorded on the SYRA station (east channel), which have been grouped into a single cluster. (d and e) AA' and BB' cross-sections, where the different event clusters are presented as a function of depth. Each colour indicates a separate cluster. In total, 19 different clusters are created with 10 (marked by the red ellipse) in close proximity to each other within the reservoir of the Reykjanes geothermal field.

P- and S-wave picks compared with manual picking. In total, about 50% less P- and S-wave picks have been determined by the automatic picking compared with the manual processing. This can be explained by the often emergent character of the P-wave onsets, which results in smaller SNRs than our defined threshold. In cases where we could not assign a P-wave onset, we did not attempt to identify S-wave onsets.

Analysis of P- and S-wave accuracy

The P- and S-wave pick consistency plays a significant part in the event location quality. We define the picking accuracy as the time difference between the automatic and the manual picks at station i :

$$\Delta t_{i, \text{accuracy}}^k = t_{i, \text{manual}}^k - t_{i, \text{automatic}}^k \quad (7)$$

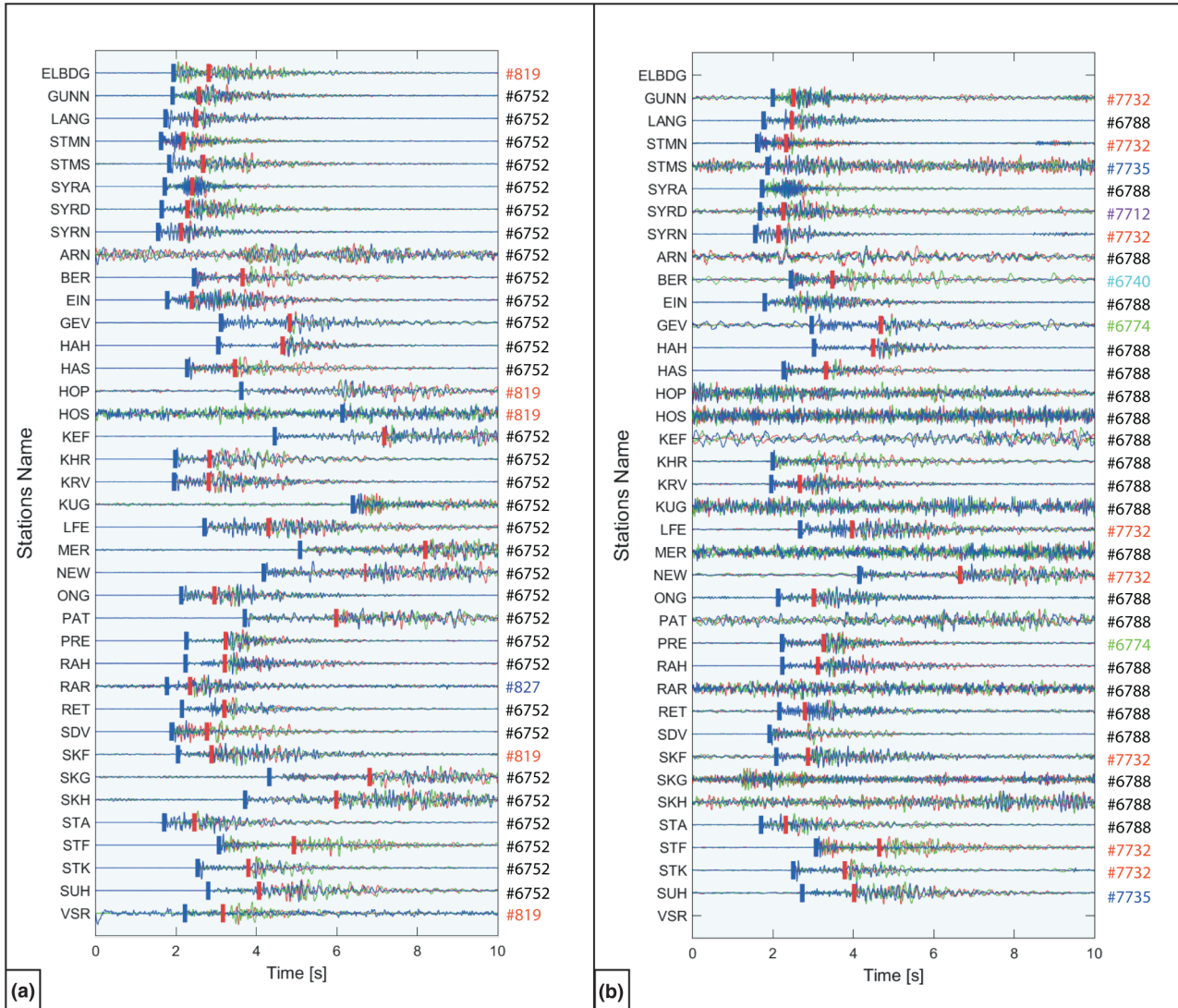


Figure 6 Example of two ATs. (a) An AT, which has 37 P-picks and 35 S-picks. It is built from the cluster shown in Fig. 5c and mainly composed of traces from a single event (#6752). However, four traces are used from event #819 and one event from #827. (b) A second AT, with less P- and S-phases picked than (a). It is composed of seven different events, predominantly event #6788.

where k is either a P- or S-wave phase. The observed pick distributions are almost Gaussian with close to zero mean (Fig. 8c, d). Approximately two-thirds of the automatic picks have an accuracy within the range of the manual picking uncertainty (100 and 200 ms; Table 2).

We compare the mean P- and S-wave pick differences for each event by averaging over all stations:

$$\Delta t_{EV, \text{accuracy}}^k = \frac{\sum_{i=0}^N (t_{\text{manual}}^k - t_{\text{automatic}}^k)}{N}, \quad (8)$$

where k is either a P- or S-wave phase, i is the station, and N is the maximum number of stations (Fig. 8e, f). As previously ob-

served, the pick distributions are Gaussian with close to zero mean. The mean P- and S-wave picks per event show that 47% and 29% of the events have an accuracy of less than 100 ms. Thus, the average time accuracy per event is higher than at the individual stations (Table 2). This can be explained by (1) the manually and automatically picked stations might differ for the same event, or/and (2) the picking accuracy varies from station to station within one event.

As a preliminary conclusion, most of the automatic picks have a high degree of accuracy but $\sim 2\%$ show rather high errors (± 1 s). In order to exclude potential mis-locations based on those few, but inaccurate, phase picks, we studied how both

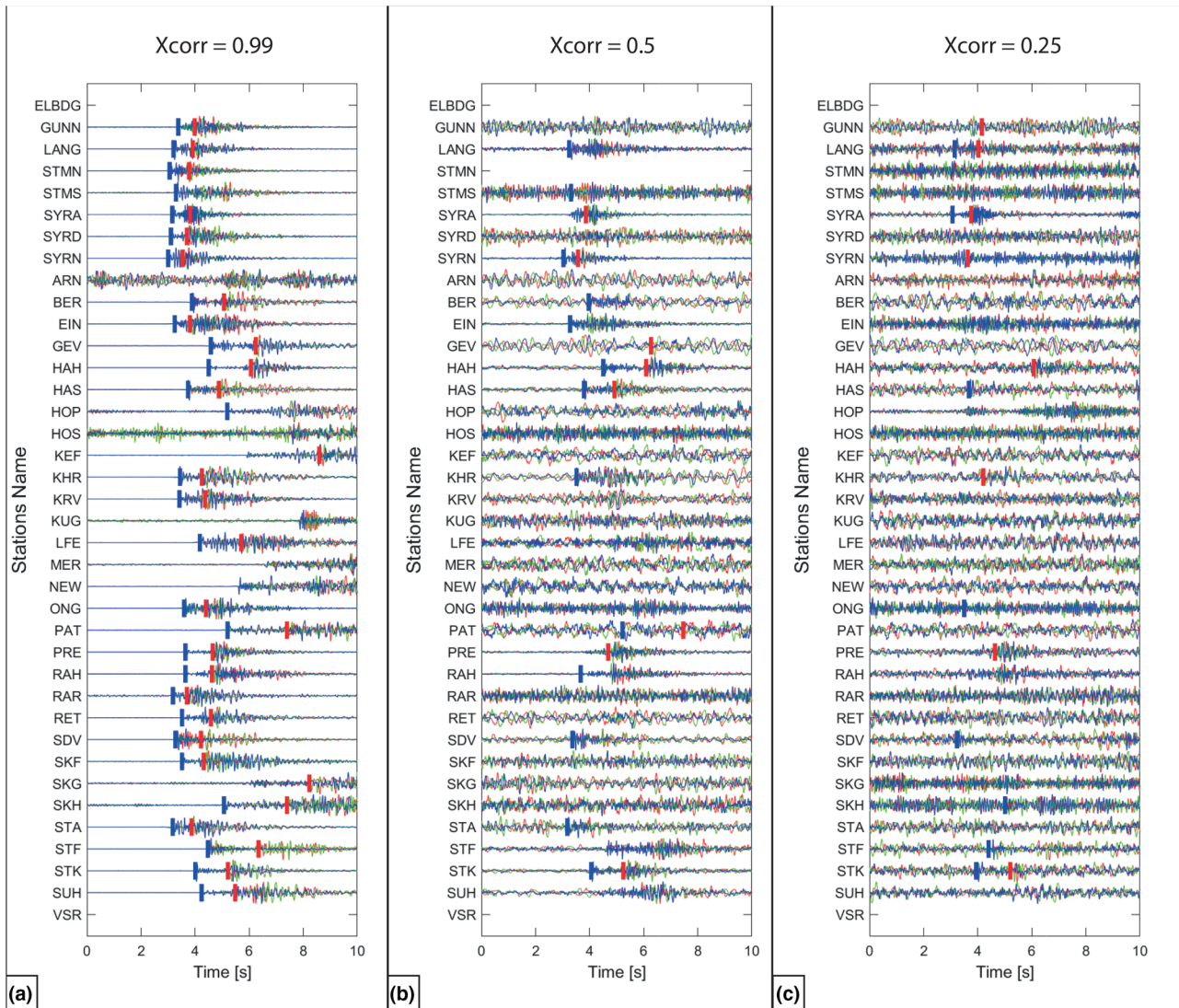


Figure 7 Example of three automatically picked child events using the AT in Figure 4(a). The mean cross-correlation coefficient between the child events and the AT varies between 0.25 and 0.99. The blue and orange vertical lines represent the P- and S-picks, respectively. (a) Event with a high SNR. P- and S-phases are well identified and picked. (b and c) Events with a lower SNR; a lot of noise contaminates these events. However, the mean cross-correlation coefficient is of 0.5 (b) and 0.25 (c). Some stations can be automatically picked even if the P and S-phases are clearly difficult to identify.

the percentage of picks and the average cross-correlation coefficient, computed between the child event and the AT, might influence the automatic picking accuracy.

Accuracy dependency on the number of picks and the cross-correlation coefficient

The AT methodology is based on waveform similarity, where the selected AT for a particular child event is determined by the average cross-correlation coefficient. For our data set, we

used a value of eight stations for computing the average cross-correlation coefficient (see Section II.C.a) since this represents the number of stations that are most frequently operational within the data set.

Even though a subset of child events can have a high mean cross-correlation coefficient (> 0.6) and a high pick accuracy, the full set of child events may still be characterized by a low mean cross-correlation coefficient (< 0.35 ; Fig. 8g, h). Such a low coefficient is obtained despite P- and S-phases only being picked when cross-correlation coefficients at individual

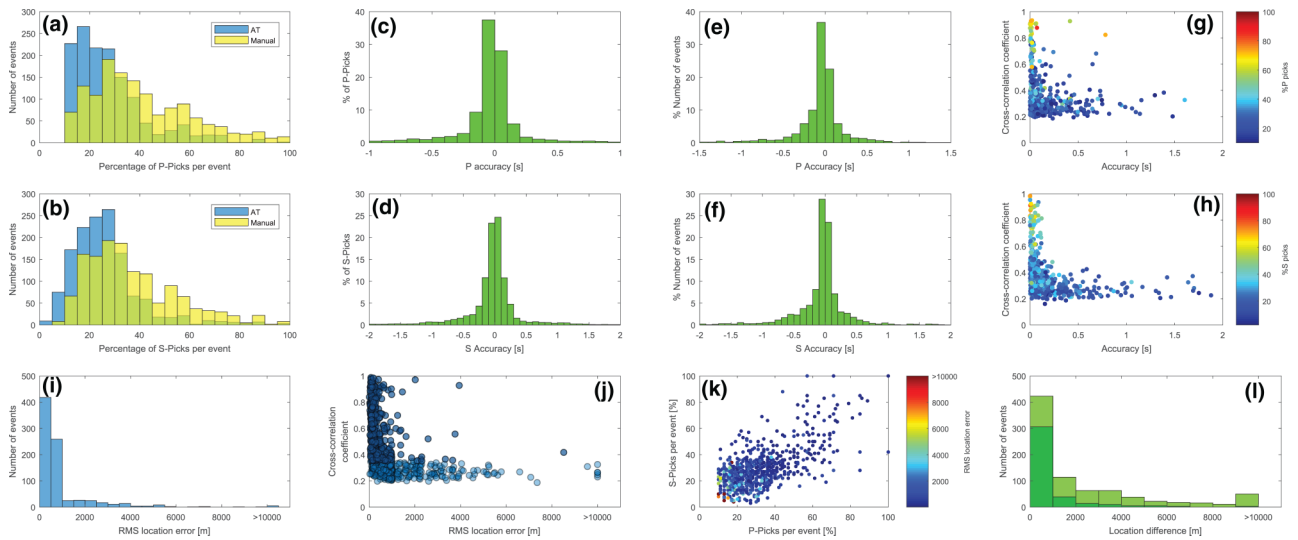


Figure 8 Analysis of the AT automatic P- and S-picking accuracy (a–h) and event locations (i–l). (a and b) The distribution of the P- and S-percentage picks for AT (blue) and manual (yellow) methods. (c and d) The accuracy of P- and S-picks per station. (e and f) Histograms of the P- and S-accuracy averaging per event. (g and h) Evolution of the average cross-correlation coefficient between each couple (event, AT) in function of the P- and S-accuracy and coloured by the percentage of P- and S-picks per event. (i) Histogram of rms location error. (j) The evolution of the mean cross-correlation coefficient as a function of the rms location error. The light blue dots indicate all the events, whereas the dark blue dots represent events with a mean cross-correlation coefficient greater than 0.35 and an rms location error lower than 1000 m. (k) Evolution of the rms location error (colours) as a function of the percentage of P- and S-phases picked per event. (l) The distance difference between the manually and automatically picked events. The light green coloured histogram uses all events, whereas the dark green histogram shows events with a mean cross-correlation coefficient greater than 0.35 and an rms location error lower than 1000 m.

Table 2 Arrival time accuracy by comparing the (AT automatic and manual) P- and S-wave picks and the (ME automatic and manual) P- and S-wave picks. The range from [−100 to 100] ms and [−200 to 200] ms is chosen to match the estimated manual picking uncertainty ranges

	P-wave picks from		S-wave picks from		Mean P per single event from		Mean S per single event from	
	EAT	ME	EAT	ME	EAT	ME	EAT	ME
t_{accuracy}^k [−100; 100] ms	66%	64%	49%	57%	47%	49%	29%	40%
t_{accuracy}^k [−200; 200] ms	81%	82%	70%	76%	69%	69%	54%	65%
t_{accuracy}^k [−1; 1] s	98%	96%	95%	96%	97%	94%	95%	93%

traces are greater than 0.75 and 0.7, respectively. What appears as a discrepancy can be explained by low SNR seismic traces, which do not contain picks, contributing to a lower mean cross-correlation coefficient. Thus, events with a low average cross-correlation coefficient will still contain high cross-correlation values for individual traces. Consequently, events with a low average cross-correlation coefficient are not indicative of inaccurate picking. The evolution of P- and S-wave pick percentages per event versus the mean cross-correlation and time accuracy (Fig. 8g, h) confirms this. The events with the smallest percentages of P- and S-wave picks are associated with the smallest cross-correlation coefficients

and typically the highest pick uncertainties. In contrast, events characterized by a high percentage of P- and S-wave picks (>40%) present a relatively high cross-correlation coefficient (>0.6) and high accuracy (<0.2 s).

To sum up, events with a mean cross-correlation greater than 0.35 or with at least 40% of their P- and S-wave phases picked show high picking accuracy, making them good candidates for event location. Below these thresholds, many events also show high picking accuracy, but there are also examples with inaccurate picks, which would potentially bias any location procedure. For such events, we recommend a manual quality checking of the automatic picking, before locating.

Location from the automatic picking

In this section, we compare the event locations obtained from the automatic and manual picking. For studying the accuracy of automatically picked event locations, we compare them to the locations derived from the manual picking. Since these events require high SNR, their locations are considered relatively reliable and are a good benchmark for the comparison. The location is performed using a differential evolution algorithm (Storn and Price, 1997; Wuestefeld *et al.*, 2018) for manually picked events with more than 30% and 20% of their P- and S-wave phases picked, respectively. The location uncertainty is quantified by the rms location error, defined as:

$$\text{rms error} = \sqrt{\frac{1}{3} (x^2 + y^2 + z^2)}, \quad (9)$$

where x , y and z are the components of the location error in Cartesian coordinates (east, north and depth) of the considered seismic event. The location errors are estimated from an error ellipsoid which quantifies how close or far the solution (measured observation) is from the prediction (theory). Only events having an rms location error lower than 1000 m are hereafter considered. Applying the same differential evolution algorithm to the automatically picked events leads to the comparison of 823 seismic event locations.

Six hundred and seventy-seven automatically picked events (i.e. 82%) give an rms location error lower than 1000 m (Fig. 8i). Fewer than 1% of events have an uncertainty of 10,000 m or greater and are excluded from this study. Events with the highest average cross-correlation values with the AT also result in the smallest location errors (< 1000 m; Fig. 8j). In the same way, most of the poorly located events are characterized by a low (<0.35) cross-correlation coefficient. Although this observation demonstrates a link between location error and the average cross-correlation coefficient value, many events with a low cross-correlation coefficient are also characterized by a small rms location error (Fig. 8j). The previous cross-correlation threshold of 0.35 is apparent and delineates two different trends in the location accuracy. For values of cross-correlation greater than 0.35, the location error is consistently small; but below this threshold, the location accuracy has a large range with no apparent upper or lower limit. We previously showed that the cross-correlation coefficient is linked to the percentage of P- and S-wave picks per event. Since the worst and best location errors are derived from events with the smallest (<40%) and highest pick percentages (Fig. 8k), respectively, we can assert that either a cross-correlation coefficient greater than 0.35

and/or 40% of picks per events will ensure a good event location.

Considering the location uncertainty on the manually and automatically picked events, Fig. 8(l) presents the minimum location difference between the reference (manual picking) events and the AT-derived automatically picked events (light green histogram). More than 55% of the events show a location difference less than 1000 m but some reach a difference as large as 10 km. By only considering events with a cross-correlation higher than 0.35 (dark green histogram), 80% of the event locations have less than 1000 m of difference compared with the reference events. Since we selected manual events with an rms location error of less than 1000 m, they are therefore within the location error of these events. In addition, events with the largest distance offset from the reference locations are also removed when the cross-correlation coefficient is above 0.35.

Thus, the AT automatic picking methodology shows a systematic link between good picks and high location accuracy when the (AT; child event) couple has a cross-correlation greater than 0.35. Below this value, manual checking is necessary to modify or remove automatic picks.

DISCUSSION

The aggregated template (AT) methodology has been developed to improve the number of locatable events and to decrease the processing time in challenging data sets by identifying the P- and S-wave onsets through template matching. Although a template matching approach using master events has already been successfully used on large microseismic data sets with a template composed of real seismic events (Rowe *et al.*, 2002), the AT concept is an innovation. To demonstrate the benefits of the AT methodology, we tested the performance of the ATs compared with the master event (ME) templates. Based on our knowledge of the Reykjanes data set, we were able to identify eight events that could be used as MEs which were well distributed along the peninsula. Based on these templates, we then repicked the previous 2160 manually picked events.

Master Event automatic pick results, manual picking and Aggregated Template comparison

In this section, we conduct a similar analysis as performed to compare the AT-derived picks with the manually derived picks (AT/manual), but instead we compare the ME automatic

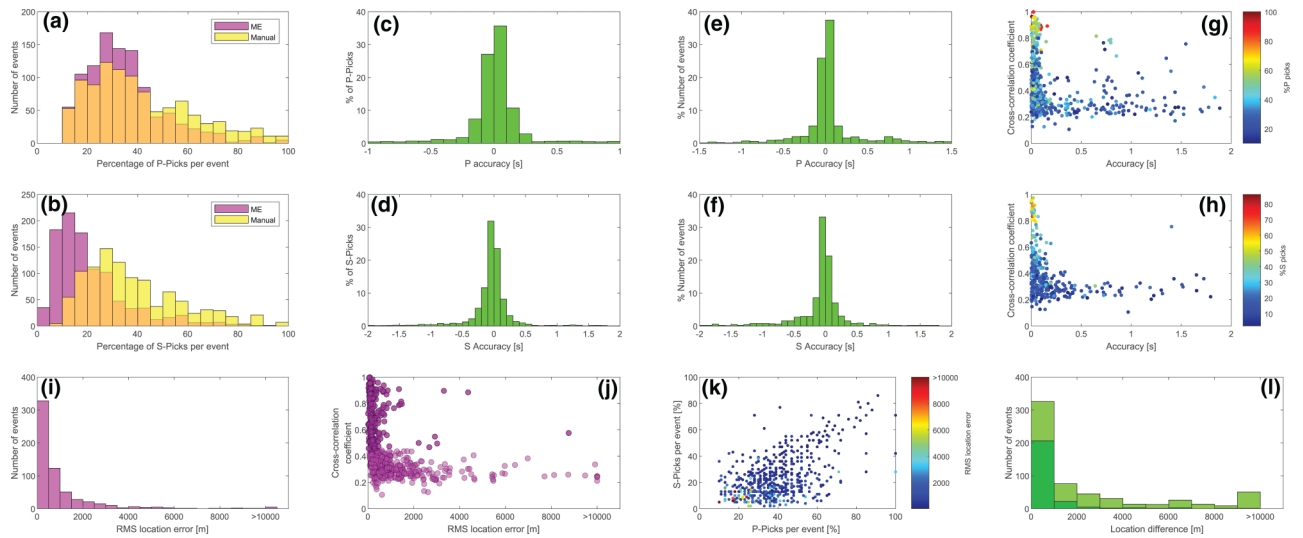


Figure 9 Analysis of the ME automatic P- and S-picking accuracy (a–h) and event locations (i–l). (a and b) The distribution of the P- and S-percentage picks for ME (pink) and manual (yellow) methods. Orange colour indicates when both methods have the same percentage picks and results for the superimposition of AT and ME. (c and d) The accuracy of P- and S-picks per station. (e and f) Histograms of the P- and S-accuracy averaging per event. (g and h) The evolution of the average cross-correlation coefficient between each couple (event, ME) as a function of the P- and S-accuracy and coloured by the percentage of P- and S-picks per event. (i) A histogram of rms location error. (j) The evolution of the mean cross-correlation coefficient as a function of the rms location error. The light pink dots indicate all the events, whereas the dark pink dots represent events with a mean cross-correlation coefficient greater than 0.45 and an rms location error lower than 1000 m. (k) The evolution of the rms location error (colour bar) as a function of the percentage of P- and S-phases picked per event. (l) The distance difference between the manually and automatically picked events. The light green coloured histogram uses all events, whereas the dark green histogram shows events with a mean cross-correlation coefficient greater than 0.35 and an rms location error lower than 1000 m.

picking with the manual picking (ME/manual). Thereafter, we will directly compare ME/manual with AT/manual picking.

Using the eight ME templates, it was possible to pick 1007 events with at least four P- and one S-wave picks, i.e. 25% less than using the AT. The ME automatic and manual P-wave pick percentage distributions (Fig. 9a) show the same trend, despite fewer events having a high P-wave pick percentage for the ME processing compared with the manually picked events. In addition, above 25% of the picks per event, ME and AT P-wave pick percentage trends (Fig. 8a) are similar despite the ME templates being more efficient at picking P-wave onsets (85% versus 50%). The ME S-pick distribution (Fig. 9b) differs from the manual picking when the pick percentage is less than 20%. Above this value, both trends are similar (as observed for the AT results). Approximately 54% of the S-picks are found with the ME automatic picking, similar to the 50% obtained with the AT picking.

The station-based and event-based pick accuracies (Fig. 9c–f) indicate most of the ME picks have less than 0.2 s difference with the manual picks (Table 2). Although the accuracy of the P-wave picks (Fig. 9c, e) is similar to those ob-

tained from the AT picks, the accuracy of the S-picks (Fig. 9d, f) demonstrates some differences. In particular, using the ME method there are 8% more events with an accuracy better than 100 ms and 3% more events with an accuracy worse than 1 s compared with the AT picking results. Similar to the AT picks (Fig. 8g, h), Figure 9(g, h) underlines that a low average cross-correlation coefficient is not indicative of inaccurate picking for the ME picks.

In summary, the ATs allow more events to be picked with an identical number of S-onsets but less P-wave phases than the ME templates. P-wave picks show a similar accuracy for both templates while S-wave picks can be both more (<200 ms) or less accurate (> 1 s).

The previously used differential evolution location algorithm is then applied and leads to the comparison of 610 ME and manually picked event locations (Fig. 9i). This represents 25% less than with ATs, which is the same value as the difference between the ME- and AT-picked events (see above). Seventy-four per cent (82% for the AT results) have an rms location error less than 1000 m (Fig. 9i) and less than 1% (same for the AT results) of the ME-picked events have an error greater than 10,000 m.

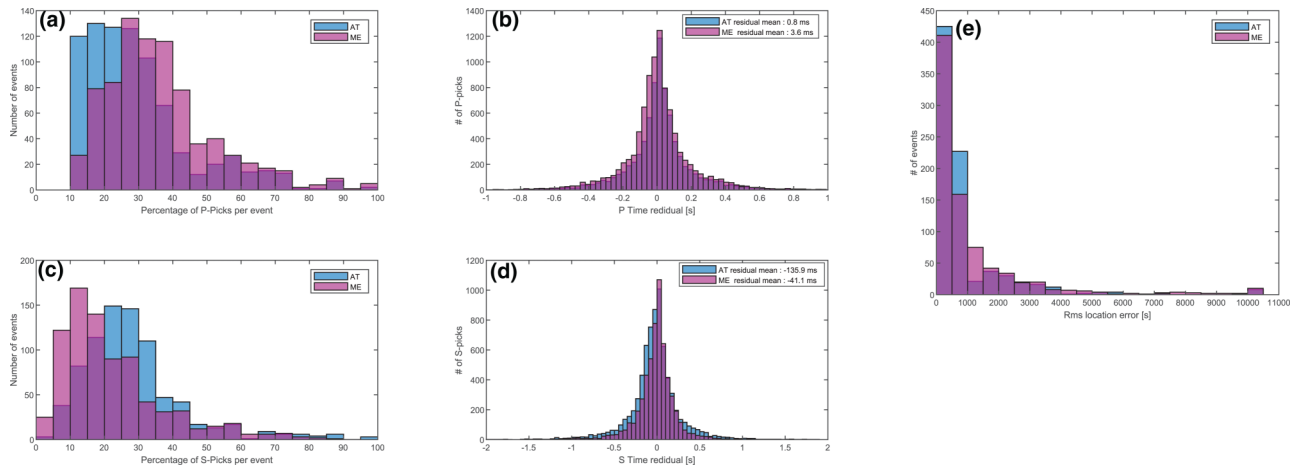


Figure 10 Comparison between the AT (blue) and the ME (pink) automatic picks. (a) P-pick and (b) S-pick percentage distributions per event. (b, d) P- and S-picks time residuals. (e) Rms location errors for AT and ME.

Both the cross-correlation coefficient (Fig. 9j) and the percentage of P- and S-wave picks (Fig. 9k) versus the rms location error show a similar trend to the AT results. Above a cross-correlation coefficient threshold (here 0.45), most of the events show a small location error (lower than 1000 m) whereas below this value, the location error can be either large or small. Thus, the trend is identical to what we observed with AT but for an average cross-correlation of 0.45 instead of 0.35. The use of the ATs is likely to artificially decrease the average cross-correlation coefficient due to the lower number of identified P-wave phases. As most of the P-wave picks are identified with the ME templates, the average cross-correlation coefficient should be more realistic of the event similarity. Finally, the minimum location difference between manual and ME-picked events shows the same tendency as the AT/manual comparison but with more events having higher offset distances (Fig. 9l).

Comparison of Master Event-picked and Aggregated Template-picked events

After comparing both the AT and ME automatic picking results with the manual picking, we now directly compare the AT and ME automatic picking results. We identified 813 events both picked with AT and ME templates.

The distribution of AT and ME P-wave pick percentages per event is similar, above 25% (Fig. 10a), even though more ME-picked events have higher P-wave pick percentages than those derived from the AT methodology. Below this 25% threshold, many more AT-picked events have smaller P-wave pick percentages, compared with the ME template re-

sults. Thus, more P-wave picks are identified through the ME method than the AT methodology. Conversely, for the S-pick distribution (Fig. 10c), more AT-picked events have higher S-pick percentages than for the ME, despite a similar distribution above 25%.

The time residual (Δt) is defined as follows: $\Delta t = t_{\text{obs}}^k - t_{\text{th}}^k$, where k is either a P- or S-wave phase, t_{obs} is the automatically picked time, and t_{th} is the theoretical time obtained from the derived event location. In comparing residuals from the two automatic picking methods, both distributions are Gaussian (Fig. 10b, d). The mean P-residual obtained from the AT picks is smaller (0.8 ms) than that obtained from the ME picking (3.6 ms). In addition, for both methods, the mean P-pick residual is positive, meaning the automatic P-wave onsets are delayed compared with the theoretical time. Conversely, the mean ME and AT S-wave picks are negative, suggesting automatic picks are picked earlier in comparison to the theoretical arrival times. The S-residual values are higher than the P-residuals, highlighting the larger pick uncertainty on the S-wave onsets compared with the P.

As shown with the AT/manual and ME/manual comparisons, more events picked using the AT methodology (Fig. 10e) have a smaller rms location error than using the ME template (80% versus 70% with errors lower than 1000 m). Thus, when the same events are picked, the AT method gives slightly better results than the classical ME method. The comparison with the manual picking has also shown that the use of MEs also gives good results. They enable the picking of events coming from areas where no AT can be defined. MEs could therefore be used to augment ATs to ensure improved coverage of the study area.

CONCLUSION

We have developed an aggregated template (AT) concept in order to perform automatic P- and S-phase picking for the case of a large and complex database with a temporally varying network. We defined an AT as a representative event for a small area, built by aggregating the best signal-to-noise ratio seismic traces from events with similar waveforms. ATs are then used similarly to master events (ME). A template matching procedure, using the AT, is applied to unpicked events to detect the P- and S-wave onsets. We tested this method on a database composed of 2160 induced events recorded by a varying number of seismic stations in the Reykjanes geothermal field (Iceland). The definition of 19 ATs enabled the automatic picking of ~65% of this database, with 70% of the identified P- and S-wave picks having an accuracy within the estimated manual picking uncertainty. We identified two main criteria for the autopicking quality: the average cross-correlation coefficient defined between an AT and a child event and the number of P- and S-wave picks. Thus, all child events with a 0.35 cross-correlation coefficient (or/and 40% of P- and S-wave picks per event) can be directly located without any manual quality checks of the arrival time picks. Below these two thresholds, we recommend a manual quality control. By comparing with the use of classical MEs, we note that ATs allow more events to be automatically picked, albeit with fewer P-wave phases. However, these P-wave phases are picked with a similar precision between the AT and ME methods. For regions where only single events occur, an AT can be directly created from this single event, i.e. using the ME as an AT. For regions where no previously recorded seismicity has occurred, an AT cannot be initially generated. With the onset of new seismicity in such a region, the set of available ATs can be updated. Finally, the AT concept also enables a significant reduction in computation time relative to traditional template matching by only using the most representative template for a region and thus limiting the required number of templates.

ACKNOWLEDGEMENTS


We thank the Research Council of Norway for funding through the ERIS project, grant #267908 and Inga Berre, project lead from the University of Bergen, Norway. We also thank ÍSOR (Iceland) for access to the seismological data, partly acquired through the EU FP7 project IMAGE.

DATA AVAILABILITY STATEMENT

The seismic data from the IM network used in this study are described by Jousset *et al.* (2020) and can be accessed through

the frame of GEOFON (<https://geofon.gfz-potsdam.de/doi/network/4L/2014>). The seismic data from the HSO network used in this study are owned by HS Orka. Data are available on request to the corresponding author with permission through HS Orka.

ORCID

Laure Duboeuf  <https://orcid.org/0000-0001-6371-3022>

REFERENCES

- Björnsson, S. and Einarsson, P. (1974) Seismicity of Iceland. In L. Kristjansson (Ed.) *Geodynamics of Iceland and the North Atlantic Area*. Dordrecht: Springer Netherlands, pp. 225–239.
- Blanck, H., Jousset, P., Hersir, G.P., Ágústsson, K. and Flóvenz, Ó.G. (2019) Analysis of 2014–2015 on- and off-shore passive seismic data on the Reykjanes Peninsula, SW Iceland. *Journal of Volcanology and Geothermal Research*, 391, 106548. <https://doi.org/10.1016/j.jvolgeores.2019.02.001>
- Bourouis, S. and Bernard, P. (2007) Evidence for coupled seismic and aseismic fault slip during water injection in the geothermal site of Soultz (France), and implications for seismogenic transients. *Geophysical Journal International*, 169(2), 723–732. <https://doi.org/10.1111/j.1365-246X.2006.03325.x>
- Cuenot, N., Dorbath, C. and Dorbath, L. (2008) Analysis of the microseismicity induced by fluid injections at the EGS Site of Soultz-sous-Forêts (Alsace, France): Implications for the characterization of the geothermal reservoir properties. *Pure and Applied Geophysics*, 165(5), 797–828. <https://doi.org/10.1007/s00024-008-0335-7>
- De Meersman, K., Kendall, J.-M. and van der Baan, M. (2009) The 1998 Valhall microseismic data set: an integrated study of relocated sources, seismic multiplets, and S-wave splitting. *Geophysics*, 74(5), B183–B195. <https://doi.org/10.1190/1.3205028>
- Deichmann, N., Kraft, T. and Evans, K.F. (2014) Identification of faults activated during the stimulation of the Basel geothermal project from cluster analysis and focal mechanisms of the larger magnitude events. *Geothermics*, 52, 84–97. <https://doi.org/10.1016/j.geothermics.2014.04.001>
- Ellsworth, W. (2013) Injection-induced earthquakes. *Science*, 341(6142), 1225942. <https://doi.org/10.1126/science.1225942>
- Ellsworth, W., Llenos, A.L., McGarr, A., Michael, A.J., Rubinstein, J.L., Mueller, C.S., *et al.* (2015) Increasing seismicity in the U.S. mid-continent: implications for earthquake hazard. *The Leading Edge*, 34(6), 618–626. <https://doi.org/10.1190/tle34060618.1>
- Foulger, G.R., Wilson, M.P., Gluyas, J.G., Davies, R.J. and Julian, B. (2018) Global review of human-induced earthquakes. *Earth-Science Reviews*, 178, 438–514. <https://doi.org/10.1016/j.earscirev.2017.07.008>
- Gaucher, E., Schoenball, M., Heidbach, O., Zang, A., Fokker, P.A., van Wees, J.D. and Kohl, T. (2015) Induced seismicity in geothermal reservoirs: a review of forecasting approaches. *Renewable and Sustainable Energy Reviews*, 52, 1473–1490. <https://doi.org/10.1016/j.rser.2015.08.026>

- Geiger, L. (1910) Herbsetimmung bei Erdbeben aus den Ankunftszeiten. *K. Gessell. Will. Goett*, 4, 331–349.
- Geiger, L. (1912) Probability method for the determination of earthquake epilefts from the arrival time only. *Bulletin St. Louis University*, 8, 60–71.
- Gibbons, S.J. and Ringdal, F. (2006) The detection of low magnitude seismic events using array-based waveform correlation. *Geophysical Journal International*, 165(1), 149–166. <https://doi.org/10.1111/j.1365-246X.2006.02865.x>
- Goertz-Allmann, B.P., Kühn, D., Oye, V., Bohloli, B. and Aker, E. (2014) Combining microseismic and geomechanical observations to interpret storage integrity at the In Salah CCS site. *Geophysical Journal International*, 198(1), 447–461. <https://doi.org/10.1093/gji/ggu010>
- Goertz-Allmann, B.P., Gibbons, S.J., Oye, V., Bauer, R. and Will, R. (2017) Characterization of induced seismicity patterns derived from internal structure in event clusters. *Journal of Geophysical Research: Solid Earth*, 122(5), 3875–3894. <https://doi.org/10.1002/2016JB013731>
- Gudhnason, E.Á. (2014) *Analysis of seismic activity on the western part of the Reykjanes Peninsula*, SW Iceland, December 2008–May 2009 (Master's thesis, Faculty of Earth Sciences, University of Iceland, p. 83).
- Jakobsdóttir, S.S. (2008) Seismicity in Iceland: 1994–2007. *Jökull*, 58, 75–100.
- Jousset, P., Blanck, H., Franke, S., Metz, M., Ágústsson, K., Verdel, A., et al. (2016) Seismic tomography in Reykjanes, SW Iceland. *Extended Abstract European Geothermal Congress, Strasbourg*.
- Jousset, P., Hersir, G.P., Blanck, H., Kirk, H., Erbas, K., Hensch, M., et al. (2020) IMAGE (Integrated Methods for Advanced Geothermal Exploration). Deutsches GeoForschungsZentrum GFZ. Other/Seismic Network. <https://doi.org/10.14470/9Y7569325908>
- Khodayar, M., Björnsson, S., Gudhnason, E.Á., Nielsson, S., Axelson, G. and Hickson, C. (2018) Tectonic control of the Reykjanes geothermal field in the oblique rift of SW Iceland: from regional to reservoir scales. *Open Journal of Geology*, 8(3), 333–382. <https://doi.org/10.4236/ojg.2018.83021>
- Kraft, T. and Deichmann, N. (2014) High-precision relocation and focal mechanism of the injection-induced seismicity at the Basel EGS. *Geothermics*, 52, 59–73. <https://doi.org/10.1016/j.geothermics.2014.05.014>
- Majer, E.L., Baria, R., Stark, M., Oates, S.J., Bommer, J., Smith, B. and Asanuma, H. (2007) Induced seismicity associated with enhanced geothermal systems. *Geothermics*, 36(3), 185–222. <https://doi.org/10.1016/j.geothermics.2007.03.003>
- Pavlis, G.L. (1992) Appraising relative earthquake location errors. *Bulletin of the Seismological Society of America*, 82(2), 836–859.
- Ross, Z.E. and Ben-Zion, Y. (2014) Automatic picking of direct P, S seismic phases and fault zone head waves. *Geophysical Journal International*, 199(1), 368–381. <https://doi.org/10.1093/gji/ggu267>
- Rowe, C.A., Aster, R.C., Phillips, W.S., Jones, R.H., Borchers, B. and Fehler, M.C. (2002) Using automated, high-precision repicking to improve delineation of microseismic structures at the Soultz geothermal reservoir. In Trifu, C.I. (Ed.) *The Mechanism of Induced Seismicity: Pageoph Topical Volumes*. Springer, pp. 563–596. https://doi.org/10.1007/978-3-0348-8179-1_24
- Shearer, P.M. (1997) Improving local earthquake locations using the L1 norm and waveform cross correlation: application to the Whittier Narrows, California, aftershock sequence. *Journal of Geophysical Research: Solid Earth*, 102(B4), 8269–8283. <https://doi.org/10.1029/96JB03228>
- Sleeman, R. and van Eck, T. (1999) Robust automatic P-phase picking: an on-line implementation in the analysis of broadband seismogram recordings. *Physics of the Earth and Planetary Interiors*, 113(1), 265–275. [https://doi.org/10.1016/S0031-9201\(99\)00007-2](https://doi.org/10.1016/S0031-9201(99)00007-2)
- Storn, R. and Price, K. (1997) Differential evolution – a simple and efficient heuristic for global optimization over continuous spaces. *Journal of Global Optimization*, 11(4), 341–359. <https://doi.org/10.1023/A:1008202821328>
- Stuermer, K., Kummerow, J. and Shapiro, S.A. (2011) Waveform similarity analysis at Cotton Valley, Texas. In 81st SEG Annual Meeting, San Antonio, TX, USA. *Expanded Abstract*, 1669–1673. <https://doi.org/10.1190/1.3627524>
- Stuermer, K., Kummerow, J. and Shapiro, S.A. (2012) Multiplet based extraction of geological structures. In 82nd SEG Annual Meeting, Las Vegas, Nevada, USA. *Expanded Abstracts*, 1–5. <https://doi.org/10.1190/segam2012-1048.1>
- Thordarson, T. and Larsen, G. (2007) Volcanism in Iceland in historical time: volcano types, eruption styles and eruptive history. *Journal of Geodynamics*, 43(1), 118–152. <https://doi.org/10.1016/J.JOG.2006.09.005>
- van der Baan, M. and Calixto, F.J. (2017) Human-induced seismicity and large-scale hydrocarbon production in the USA and Canada. *Geochemistry, Geophysics, Geosystems*, 18(7), 2467–2485. <https://doi.org/10.1002/2017GC006915>
- Weemstra, C., Obermann, A., Verdel, A., Paap, B., Blanck, H., Guðnason, E.Á., et al. (2016) Time-lapse seismic imaging of the Reykjanes geothermal reservoir. In Proceedings of the European Geothermal Congress. European Geothermal Energy Council (EGEC), Strasbourg.
- Wuestefeld, A., Greve, S.M., Näsholm, S.P. and Oye, V. (2018) Benchmarking earthquake location algorithms: a synthetic comparison. *Geophysics*, 83(4), KS35–KS47. <https://doi.org/10.1190/geo2017-0317.1>
- Zang, A., Oye, V., Jousset, P., Deichmann, N., Gritto, R., McGarr, A., et al. (2014) Analysis of induced seismicity in geothermal reservoirs – an overview. *Geothermics*, 52(Supplement C), 6–21. <https://doi.org/10.1016/j.geothermics.2014.06.005>